Volume 18, Number 1, 2025. pp. 81-88

Jordan Journal of Physics

ARTICLE

Performance of a Thin Layer of Plastic Scintillator Material to be Used as a Charged Particle Detector Using Geant4

K. Al-Khasawneh[a], **B. Brückner**[b], **P. Erbacher**[b], **S. Fiebiger**[b], **K. Göbel**[b], **T. Heftrich**[b], **Kisselbach**[b], **D. Kurtulgil**[b], **C. Langer**[b], **M. Reich**[b], **R. Reifarth**[b], **M. Volknandt**[b] and **M. Weigand**[b]

[a] *Jordan Atomic Energy Commission, Jordan Research and Training Reactor (JRTR), Amman, Jordan.*

[b] *Goethe University Frankfurt, Frankfurt, Germany.*

Doi: **https://doi.org/10.47011/18.1.9**

Received on: 11/10/2023; *Accepted on: 02/01/2024*

Abstract: The performance of a thin layer of plastic scintillator is investigated for use as a charged particle detector in various applications, including neutron-induced reactions with a charged particle in the exit channel. The detection efficiency for alpha particles and background radiation, including γ-radiation, electrons, and neutrons, was investigated using the Geant4 simulation toolkit. The results show that a thin layer of plastic scintillator can measure the alpha particles with a high efficiency of 50% for isotropic sources while keeping background radiation (with a very low detection efficiency) below 10%.

Keywords: Plastic Scintillator, Alpha interaction, gamma interaction.

Introduction

In the field of astrophysics, two complementary methods are extensively employed as a means of studying neutron-induced reactions with charged particles in the exit channel (n,z) reaction, the time-of-flight (ToF), and the neutron activation technique. The ToF technique is characterized by low values of neutron flux at the sample position because of the relatively long distances, typically several meters, between the neutron production target and the sample position [1.]. On the contrary, in the neutron activation technique, the sample is very close to the neutron production target and is characterized by a high neutron flux [2]. Therefore, detectors used to measure charged particles in such experiments should meet specific requirements, including high detection limits for the charged particle radiations and low detection limits for background radiation such as γ-radiation, electrons, and neutrons.

In the last few decades, gas ionization chambers have widely been used for the cross-section measurement of neutron-induced charged particle reactions [3]. The merit of this choice is the low sensitivity of these chambers to neutron radiation, which makes the counting process possible in the presence of the neutron beam. In addition, ionization chambers have the advantage of high detection efficiency. However, such detectors are difficult to operate, and the gas must be recycled to maintain the purity of the detection medium. Silicon detectors have also been investigated for (n,z) measurements. Unlike the ionization chambers, silicon detectors are very sensitive to neutron radiation and must be operated outside the neutron beam [8].

The scope of this work is to computationally test the performance of a thin layer of plastic scintillator material as a charged particle detector

Corresponding Author: Kafa Al-Khasawneh **Email**: kafa.khasawneh@jrtr.gov.jo

in an environment full of background radiation, including gamma, electrons, and neutrons. The goal is to understand its operational behavior and optimize the scintillator dimensions according to experimental conditions. In this regard, a computer simulation model based on the Geant4 simulation package (version 10.3.0) was developed and employed to investigate the energy deposition spectra for alpha particles, gamma radiation, electrons, and neutrons. This simulation was performed for different initial kinetic energies and different scintillator material thicknesses.

Geant4 Simulation Overview

Geant4 (**GE**ometry **AN**d **T**racking) is a multi-purpose object-oriented simulation toolkit developed at CERN [9]. It is used to accurately simulate particle interactions with matter across a very wide energy range using Monte Carlo methods. Nowadays, it is widely used to study the response of detectors for ionizing radiation, efficiency calculations, and radiation damage. All aspects of the simulation process are included in the toolkit, including geometry of the system, materials involved, fundamental particles of interest, generation of primary events, tracking of particles through materials and electromagnetic fields, physics processes governing particle interactions, response of sensitive detector components, generation of event data, storage of events and tracks, visualization of the detector and particle trajectories, and analysis of simulation data at different levels of detail and refinement [10].

Figure 1 shows the information flow of the simulation developed for this work. The simulation started by defining the geometry, which in this study was composed of a primary mother volume called "world" that included all the components that the simulation had to consider. The world's shape was a cube with 20 m sides. To simulate realistic conditions, the "air" material, as recommended by the U.S. National Institute of Standards and Technologies (NIST) libraries, was assigned as the world material [11]. Inside the world volume, the detector volume was defined, which was a simple parallel rectangular plastic scintillator plate.

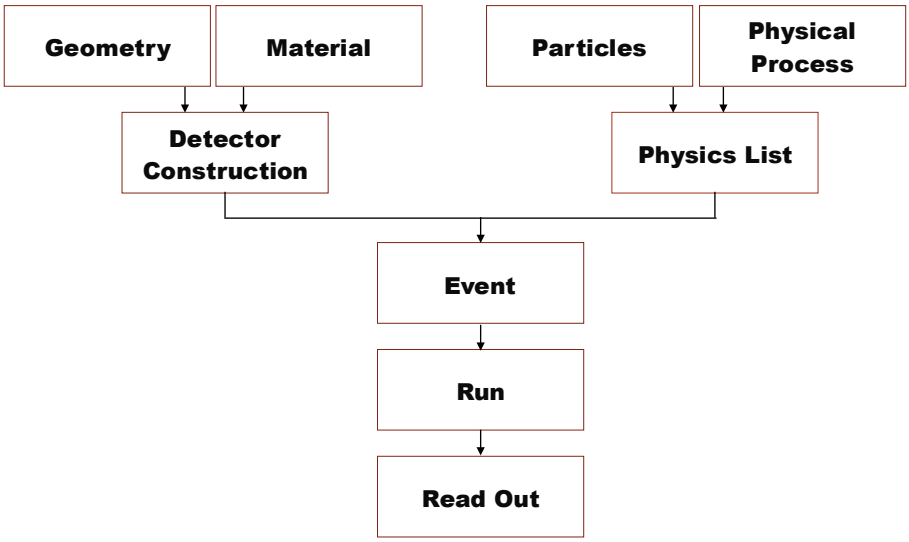

FIG. 1. Workflow diagram of the simulation program implemented in this work.

The plate had dimensions of 26 × 7 cm^2 surface area in the YZ-plane. At this stage, for comparison, different scintillator thicknesses in the X-direction were defined. The plastic scintillator material composition was determined based on its atomic number and density values. The compositions of the different materials used are summarized in Table 1.

Implementation of the primary particle generator was achieved through the use of the G4GeneralParticleSource (GPS) [12], which generates a particle beam by specifying its type, position, kinetic energy, and angular distribution. In this study, a point source with an isotropic distribution was created (see Table 1). The source was positioned at the center of the world volume, in direct contact with the scintillator volume (i.e., the distance between the point source and the scintillator plate surface was approximately 0 cm).

The physical processes considered in this simulation were the electromagnetic interactions governing energy loss for primary particles, including photons, electrons, positrons, and other charged particles.

TABLE 1. Composition and densities of the different materials used in these simulations. All particle types, shapes, and angular distributions are also given.

Geometry	Volume	Material	Composition	Density [mg/cm^3]
	World	Air	N (79%) O (21%)	1.290
	Scintillator	Polyvinyltolunene	C (91.5% H (8.5%)	1.032
Generalized Particle Source (GPS)	Particle	Type	Angular Distribution	
	Alpha	Point	Isotropic	
	Gamma	Point	Isotropic	
	Electrons	Point	Isotropic	

Geant4 provides many models for electromagnetic physical processes [13]. This simulation focused on the energy deposition of charged particles, gamma radiation, and neutrons, where a significant amount of low-energy secondary electrons are expected. The Low Energy EM package was used, as it is optimized for electrons with energies below 250 eV [14]. Once the geometry and the primary particle generator were created, the simulation was executed. In the Geant4 structure, each "run" contains a specific number of "events" that share the same geometry, physics list, and particle generator settings. Each event is composed of one or more primary particles. Once these primary particles enter the detector geometry, they undergo various interactions, generating secondary particles. All particles, both primary and secondary, were tracked within the detector volume until they either decayed, stopped, or exited the world volume. The energy deposition at each step was recorded, and only the total energy deposition in the detector volume at the end of each event was stored using the GetTotalEnergyDeposit() method.

It is worth pointing out that this simulation considered only total energy deposition without incorporating optical processes related to scintillation effects. As a result, in practical experiments, some discrepancies may arise between the experimentally measured detection efficiency and the absorption efficiency calculated in this study. These variations are primarily due to statistical fluctuations in light production and transmission, photo-multiplication, and electronic pulse processing.

Material Sensitivity to Alpha Particles

Using the described simulation model, the scintillator material's response to a beam of alpha particles was explored. For this purpose, the alpha range in the scintillator material and its full peak absorption efficiency were calculated. A prior analysis of the energy deposition spectrum produced by a beam of alpha particles is crucial to verify the reliability and validity of the physical processes implemented in the simulation and to emphasize the understanding of the energy deposition mechanism in the scintillator material.

A beam of alpha particles was emitted isotropically toward the center of a bare scintillator foil. Each alpha particle entering the scintillator undergoes simultaneous interactions with numerous orbital electrons, leading to ionization or excitation. As a result of these interactions, the particle gradually slows down and eventually comes to a stop.

Depending on the initial energy of the alpha particle, a large number of secondary electrons are generated with relatively low energies (≈ 0.25 keV). These secondary electrons undergo multiple scatterings within the scintillator volume. If all secondary electrons deposit their energy within the scintillator, the full energy of the alpha particle is deposited. However, some electrons may escape the scintillator and deposit their energy in the surrounding air, resulting in an energy deposition lower than the initial incident energy. Conversely, alpha particles originating in the air also undergo multiple scatterings due to interactions with air

molecules. As a result, a significant fraction of secondary electrons successfully deposit energy within the scintillator body.

This behavior is illustrated in Fig. 2, which presents the energy deposition spectrum of a mono-energetic beam consisting of 10^9 alpha particles. The initial energy was set to 1000 keV, and the scintillator thickness was 1 mm.

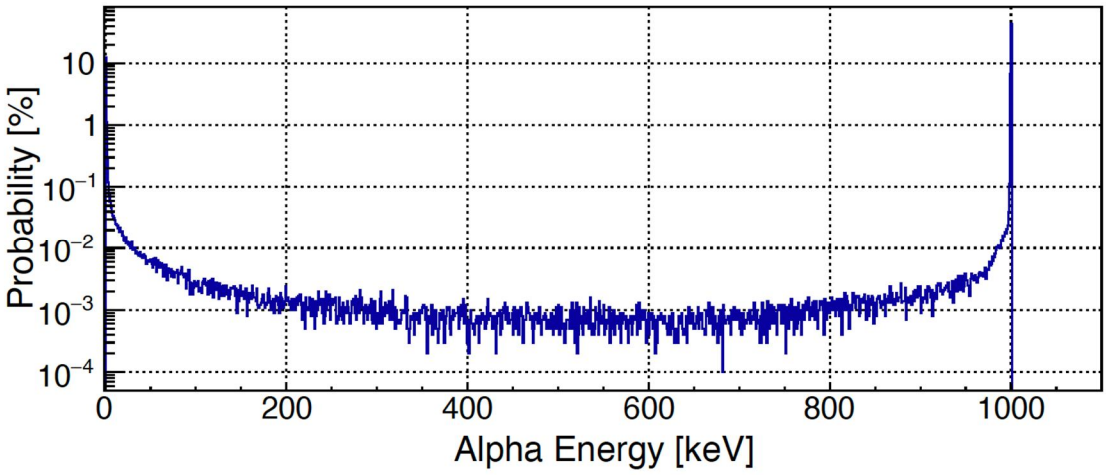

FIG. 2. Geant4-simulation of the energy deposition spectrum for a beam of 1 MeV α-particles in a 1 mm thick plastic scintillator.

Next, the proper scintillator thickness that optimizes full peak absorption efficiency was investigated. The full peak absorption efficiency is defined as the probability that an alpha particle deposits all of its initial energy in the scintillator body. For instance, an alpha particle with an initial energy of ≈ 5.5 MeV (Amaracium-241 and Polonium-210) was measured. Therefore, the alpha energy of the isotropic point source defined earlier was set to 5500 keV. This step was repeated for different scintillator thicknesses.

The full peak absorption efficiency (ε_α) was calculated as the ratio of the number of alpha events recorded under the full energy peak to the total number of alpha events originally emitted from the isotropic source, as expressed by the equation:

$$\varepsilon_\alpha = \frac{\text{Number of events under the full energy peak}}{\text{Total Number of events emitted from the source}}. \quad (1)$$

Figure 3 shows the full peak absorption efficiency as a function of scintillator thickness. As the material thickness increases, the probability of complete energy deposition also rises, leading to higher efficiency. However, this increasing trend ceases when the scintillator thickness reaches the range of alpha particles (in this example = 40 μm). At this thickness, a maximum efficiency of 50% is achieved for an isotropic source. Any further increase in scintillator thickness does not improve efficiency.

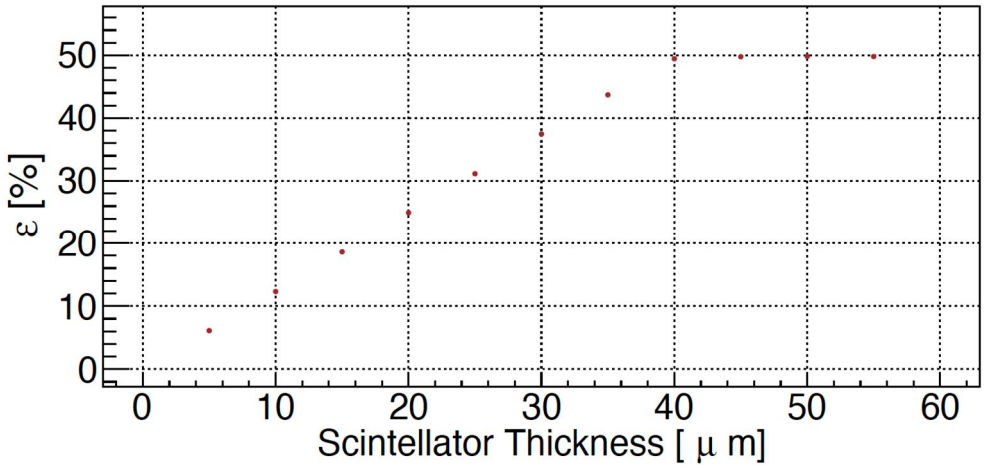

FIG. 3. Full peak absorption efficiency for a 5.5 MeV alpha particle in a scintillator material for different material thicknesses.

To determine the alpha particle's range in the scintillator material, the isotropic point source was replaced with a point source that emitted alpha particles in the scintillator direction. This was achieved using the G4GeneralParticle Source by setting the beam direction of the point source as *gps/direction 1 0 0*. This means that all the emitted particles are focused on the X-axis. Each alpha particle was tracked within the scintillator volume with a step-size of 200 nm.

During the tracking process, a production cut of 0.5 μm was implemented, meaning that once an alpha particle energy reached a value where the produced secondary particles had ranges shorter than 0.5 μm, the tracking process was terminated, and the remaining kinetic energy was deposited locally. For each event, the final stopping position (X, Y, Z) within the scintillator volume was recorded. The range value was determined as the distance between its starting and stopping points along the shooting direction (X-direction).

In low-energy nuclear physics, alpha particle energies typically fall within the multi-MeV range. Therefore, the range calculation was performed for initial alpha energies from 1 to 7 MeV in steps of 0.5 MeV.

Table 2 presents the calculated range values for different initial alpha particle energies, comparing them with values obtained from SRIM [15]. A typical relative error of ~10% was observed, attributed to the different computational approaches used in SRIM and Geant4. While SRIM employs a semi-empirical model based on interaction probabilities, Geant4 utilizes interaction cross-sections derived from direct measurements or extrapolations [9, 15].

TABLE 2. The range of an alpha particle values in the scintillator material as measured using Geant4. Values obtained from SRIM are also listed.

Alpha Energy	Range [μm]	
[keV]	Geant4	SRIM
1000	4.52	4.91
1500	6.78	7.28
2000	9.46	10.02
2500	12.56	13.15
3000	16.08	16.67
3500	20.01	20.58
4000	24.35	24.87
4500	29.10	29.54
5000	34.23	34.59
5500	39.77	40.02
6000	45.70	45.83
6500	52.00	52.01
7000	58.68	58.55

Material Sensitivity to Gamma Radiation

Due to the low effective atomic number and density of plastic scintillator material, the photoelectric effect mechanism for thin layers is not probable. Here, Compton scattering is the dominant interaction mechanism. Additionally, for layers thinner than 1 mm, the multiple scattering process is negligible, and energy deposition is due to single Compton scattering.

In Compton scattering, the produced electrons have relative energies higher than those produced by alpha particles. For instance, a 1 MeV photon produces a single electron with a maximum energy of ≈ 0.79 MeV (scattering angle = π). The range of such a high secondary electron is several orders of magnitude greater than the thickness of a thin scintillator material, making the full energy deposition improbable.

To study the effect of the material thickness on the energy deposition spectrum, an isotropic beam of monoenergetic gamma radiation of 1 MeV was directed toward the center of the scintillator. Figure 4 illustrates the energy deposition spectra for three different scintillator thicknesses: 0.04, 0.1, and 1 mm. The optimal thickness for measuring alpha particles of ≈ 5.5 MeV was determined to be 0.04 mm.

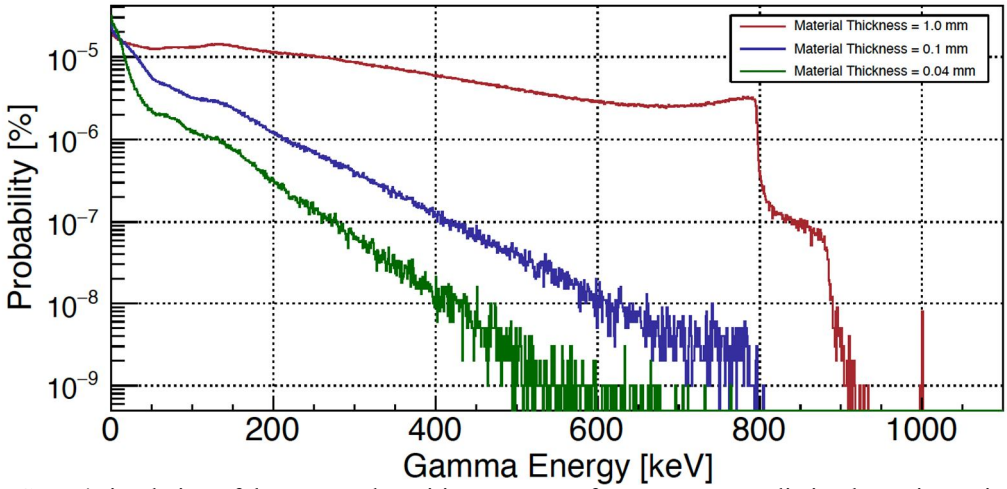

FIG. 4. Geant4 simulation of the energy deposition spectrum from a gamma radiation beam in a scintillator material with thicknesses of 1, 0.1, and 0.04 mm.

The photo-peak was observed only with a 1 mm scintillator thickness, with a very low probability (0.001 %). For thinner materials, the continuous Compton spectrum is the only distinguishing feature. The total energy deposition by secondary electrons depends on the material thickness. If the scintillator's dimensions exceed the range of the secondary electrons, these electrons will deposit their full energy within the scintillator. Otherwise, only partial energy deposition will occur.

The probability of a gamma event resulting in full or partial energy deposition within the scintillator was also examined. The simulation was conducted over an energy range of 100-2000 keV, with a step of 100 keV, for three different material thicknesses: 1, 0.1, and 0.04 mm. The total absorption efficiency for a given energy (ε_γ) was calculated as the ratio of the total number of gamma events under the full spectrum to the total number of gamma events initially emitted from the isotropic source:

$$\varepsilon_\gamma = \frac{\text{Total of events under the full spectrum}}{\text{Total Number of events emitted from the istropic source}}. \quad (2)$$

Based on this calculation, the total absorption efficiency of the gamma radiation beam is shown in Fig. 5. The first notable observation is that the total absorption efficiency is relatively low, remaining below 5%. For instance, a scintillator with a 1 mm thickness achieves an efficiency of approximately 3% for low-energy gamma rays (E = 100 keV), which sharply decreases at higher gamma energies. For a given gamma energy, total absorption efficiency strongly depends on the material thickness, with thinner materials exhibiting significantly lower absorption efficiency. For example, the total absorption efficiency for 1 MeV gamma rays was calculated to be 1.7%, 0.26%, and 0.12% for material thicknesses of 1, 0.1, and 0.04 mm, respectively.

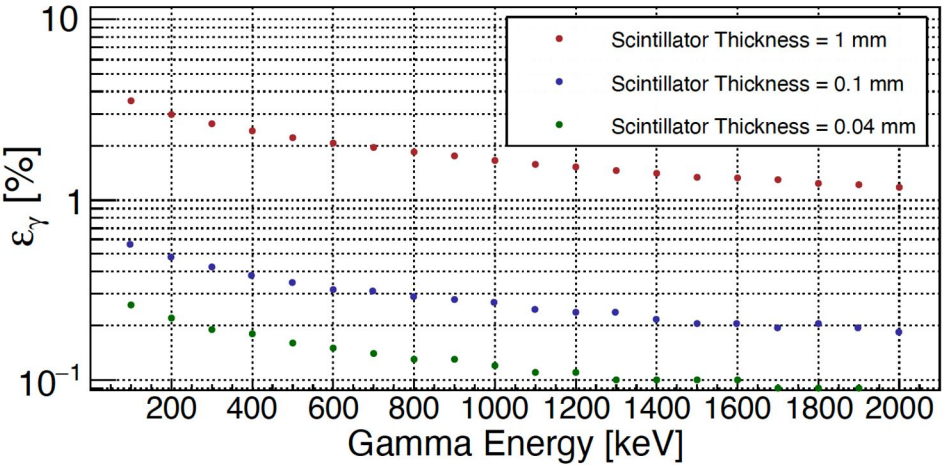

FIG. 5. Total absorption efficiency of a gamma radiation beam.

Material Sensitivity to Electrons

When electrons enter the scintillator body, they undergo elastic and inelastic scatterings with orbital electrons. As a result of these interactions, electrons lose energy and change direction. The probability of either partial or full energy deposition in the scintillator body is a function of both the electron energy and the scintillator dimensions.

To verify the effect of material thickness on total energy deposition, an isotropic beam of monoenergetic electrons was used. In this example, the initial energy was set to 389 keV (the most probable energy in the ^{210}Bi beta spectrum). The simulation was performed for three different scintillator thicknesses: 1, 0.1, and 0.04 mm.

Figure 6 presents the energy deposition spectrum. Due to multiple scattering processes within the scintillator (including surface interactions), the probability of electrons depositing their full energy is low. In this example, for a 1 mm thick scintillator, the probability of full energy deposition is approximately 30%. However, as the material thickness decreases, the deposited energy significantly decreases: for 0.1 mm thickness, the probability drops to 0.78%, and for 0.04 mm thickness, it further reduces to 0.07%. In thinner materials, electrons are more likely to undergo partial energy deposition before escaping the scintillator.

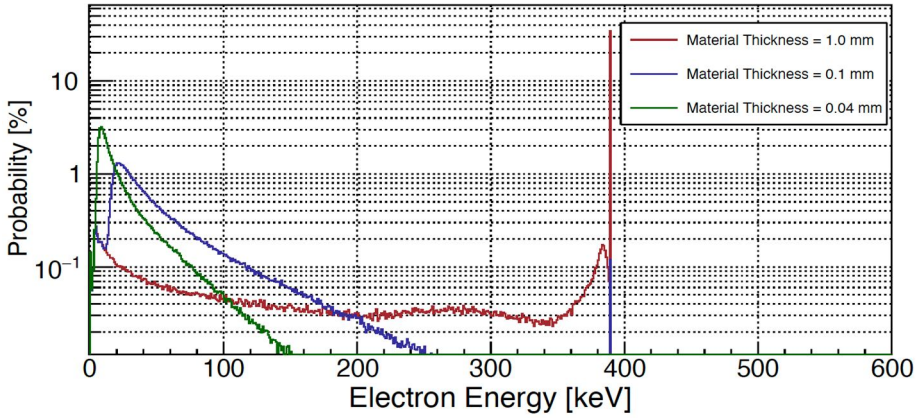

FIG. 6. Geant4 simulation of the energy deposition spectrum for a 389 keV electron beam in scintillator material with different thicknesses.

For thin scintillators, the peak observed at low energies represents the most probable energy loss, known as the Landau peak [16]. Unlike gamma radiation, decreasing the material thickness does not reduce the total absorption efficiency but rather lowers the average energy deposition by electrons. This reduction can, to some extent, decrease the light output and thus the experimental detection efficiency. However, since optical processes are not included in this study, this behavior cannot be illustrated. However, the full peak absorption efficiency for different initial electron energies, ranging from 100 to 2000 keV, was estimated and is presented in Fig. 7.

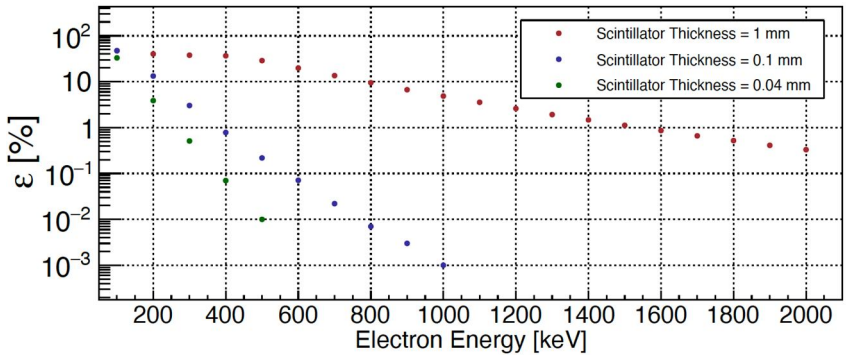

FIG. 7. Full peak absorption efficiency for electrons in a scintillator material at different electron energies and material thicknesses.

In the low-energy range, each electron that reaches the scintillator volume undergoes full energy deposition, but the energy deposited decreases for more energetic electrons because the probability of escaping is higher.

Material Sensitivity to Neutrons

Plastic scintillator materials have very low relative densities, making interactions with scattered neutrons improbable. In order to verify this, the QGSP BERT HP physics list was introduced. This physics list includes high-precision neutron tracking models and provides information about various interaction models for low-energy neutrons (≤ 20 MeV), such as elastic, inelastic, capture, and fission processes [17].

The probability of interaction with scattered neutrons was assessed using a neutron beam with energies ranging from 0.025 keV to 100 keV. The results confirmed that, given the scintillator thicknesses used in this study, neutron interactions are highly improbable.

Discussion and Conclusions

The main goal of this study is to investigate the scintillator material's response to different ionizing radiation. These materials can be used for charged particle measurement in neutron-induced reactions with charged particles in the exit channel (n,z). Based on the above simulation results, a scintillator thickness of 40 µm is sufficient for measuring alpha particles with 5 MeV, obtaining an alpha detection efficiency of 50% while maintaining a very low detection efficiency for background radiation. For instance, electrons with an energy of 389 keV exhibit a detection efficiency of just 0.07%, and gamma radiation of various energies has a detection efficiency below 10%. This work can be further improved by implementing optical processes in the plastic scintillator, allowing for a more accurate estimation of experimental detection efficiency.

Acknowledgment

Authors gratefully acknowledge the financial support by the DFG-project NICE (RE 3461/3-1).

References

[1] Reifarth, R., Lederer, C., and Käppeler, F., J. Phys. G Nucl. Part. Phys., 41 (2014) 053101.

[2] Reifarth, R., Erbacher, P., Fiebiger, S., Göbel, K., Heftrich, T., Heil, M., Käppeler, F., Klapper, N., Kurtulgil, D., Langer, C., Lederer-Woods, C., Mengoni, A., Thomas, B., Schmidt, S., Weigand, M., and Wiescher, M., Eur. Phys. J. Plus, 133 (2018) 424.

[3] Schatz, H., Jaag, S., Linker, G., Steininger, R., and Käppeler, F., Phys. Rev. C, 51 (1995) 379.

[4] Popov, Yu.P., Przytula, M., Rumi, R.F., Stempinski, M., and Frontasyeva, M., Nucl. Phys. A, 188 (1972) 212.

[5] Wilkinson, D.H., "Ionization Chambers and Counters" (Cambridge University Press, New York, 1950).

[6] Koehler, P.E., Harvey, J.A., and Hill, N.W., Nucl. Instrum. Methods Phys. Res. A, 361 (1995) 270.

[7] Goeminne, G., Wagemans, C., Wagemans, J., Serot, O., Loiselet, M., and Gaelens, M., Nucl. Phys. A, 678 (2000) 11.

[8] Woods, P.J. et al. (n_TOF Collaboration), Phys. Rev. C, 104 (2021) L032803.

[9] Geant4 Simulation Toolkit, URL: http://geant4.web.cern.ch/geant4/.

[10] Agostinelli, S., Allison, J., and Amako, K., Nucl. Instrum. Methods Phys. Res. A, 506 (2003) 250.

[11] National Institute of Standards and Technology, URL: http://www.nist.gov.

[12] Geant4 User's Guide for Application Developers, Version: Geant4 10.3,9, Geant4 Collaboration (2016).

[13] Allison, J. et al., IEEE Trans. Nucl. Sci., 53 (2006) 270.

[14] Golovko, V.V., Iacob, V.E., and Hardy, J.C., Nucl. Instrum. Methods Phys. Res. A, 594 (2) (2008) 266.

[15] Ziegler, J.F., Ziegler, M.D., and Biersak, J.P., Nucl. Instrum. Methods Phys. Res. B, 268 (2010) 1818.

[16] Aderholz, M., Lehraus, I., and Matthewson, R., Nucl. Instrum. Methods, 193 (1975) 45.

[17] Geng, C., Tang, X., Guan, F., Johns, J., Vasudevan, L., Gong, C., Shu, D., and Chen, D., Radiat. Prot. Dosim., 168 (4) (2016) 433.